C. T.-C. Nguyen, "Micromachining technologies for miniaturized communication devices," *Proceedings of SPIE*: Micromachining and Microfabrication, Santa Clara, California, Sept. 20-22, 1998, pp. 24-38.

Micromachining technologies for miniaturized communication devices

Clark T.-C. Nguyen

Center for Integrated Sensors and Circuits
Department of Electrical Engineering and Computer Science
University of Michigan
Ann Arbor, Michigan 48109-2122

ABSTRACT

An overview of the key micromachining technologies that enable communications applications for MEMS is presented with a focus on frequency-selective devices. In particular, micromechanical filters are briefly reviewed and key technologies needed to extend their frequencies into the high VHF and UHF ranges are anticipated. Series resistance in interconnect or structural materials is shown to be a common concern for virtually all RF MEMS components, from mechanical vibrating beams, to high-*Q* inductors and tunable capacitors, to switches and antennas. Environmental parasites—such as feedthrough capacitance, eddy currents, and molecular contaminants—are identified as major performance limiters for RF MEMS. Strategies for eliminating them via combinations of monolithic integration and encapsulation packaging are described.

Keywords: RF, wireless, MEMS, micromechanical, resonator, filter, inductor, capacitor, switch, communications, *Q*

1. INTRODUCTION

Due in large part to regulatory bodies, such as the Federal Communications Commission (FCC), virtually all major communication systems are based to some extent on partitioning of the electromagnetic frequency spectrum. This frequency multiplexed nature of present day communication networks naturally demands that the enabling communication transceiver devices be capable of high frequency selectivity, i.e., capable of selecting a given frequency band while rejecting all others. Thus, frequency-selective devices—filters, oscillators, and mixers—constitute some of the most important components within a transceiver, and the availability and quality of these devices often dictate the overall architecture of a given transceiver.

Unfortunately, advances in frequency-selective capabilities have lagged those for other transceiver functions, such as amplifiers or demodulation circuits, that directly benefited from the integrated circuit (IC) revolution. As a consequence, off-chip, highly selective, passive components are still used in the vast majority of today's cordless and cellular phones, forcing board-level implementation of such devices and posing a significant bottleneck against the ultimate miniaturization of portable transceivers. The lack of suitable, miniature, frequency-selective devices has also influenced the architectural evolution of transceivers towards those that maximize the application range of transistor circuitry often at the expense of performance and power dissipation. For example, although dynamic range considerations force direct-conversion receivers to consume more power than their super-heterodyne counterparts, the former are still preferred over the latter because they have more relaxed frequency selection requirements, and thus, are more amenable to implementation via transistor integration.

Fortunately, recent efforts to apply micromachining technologies to the miniaturization and integration of frequency-selective devices are starting to bring passive device technology on par with that of transistors. In particular, micromachining technologies have successfully achieved miniaturized and integrable versions of low loss, highly selective bandpass filters covering a wide range of frequencies (from 20 kHz to 90 GHz); high-*Q* inductors and tunable capacitors for voltage-controlled oscillators and matching networks; micromechanical low-loss switches for phased arrays and configurable power amplifiers; and ultra-high-*Q* resonators for stable reference oscillators. Figure 1 presents the typical block diagram for a super-heterodyne wireless transceiver, indicating the components that could greatly benefit from micromachined replacements. A more complete discussion of the specific micromachined devices applicable to communication transceivers is given in refs. 1 and 2.

This paper reviews the specific micromachining technologies that have made the above devices possible. Discussion of technology begins in Section 3 with an account of the role that polysilicon surface micromachining has played in the implementation of high-*Q* vibrating mechanical resonators and their associated applications. The resistive and *Q* deficiencies of polysilicon are also discussed in this section, providing a convenient lead in for Sections 4 and 5, which consider alternative

Additional author information:
Full Address: 2406 EECS Bldg., 1301 Beal Ave, University of Michigan, Ann Arbor, MI 48109-2122
Tel: (734)764-1220, FAX: (734)763-9324, email: ctnguyen@eecs.umich.edu, http://www.eecs.umich.edu/~ctnguyen

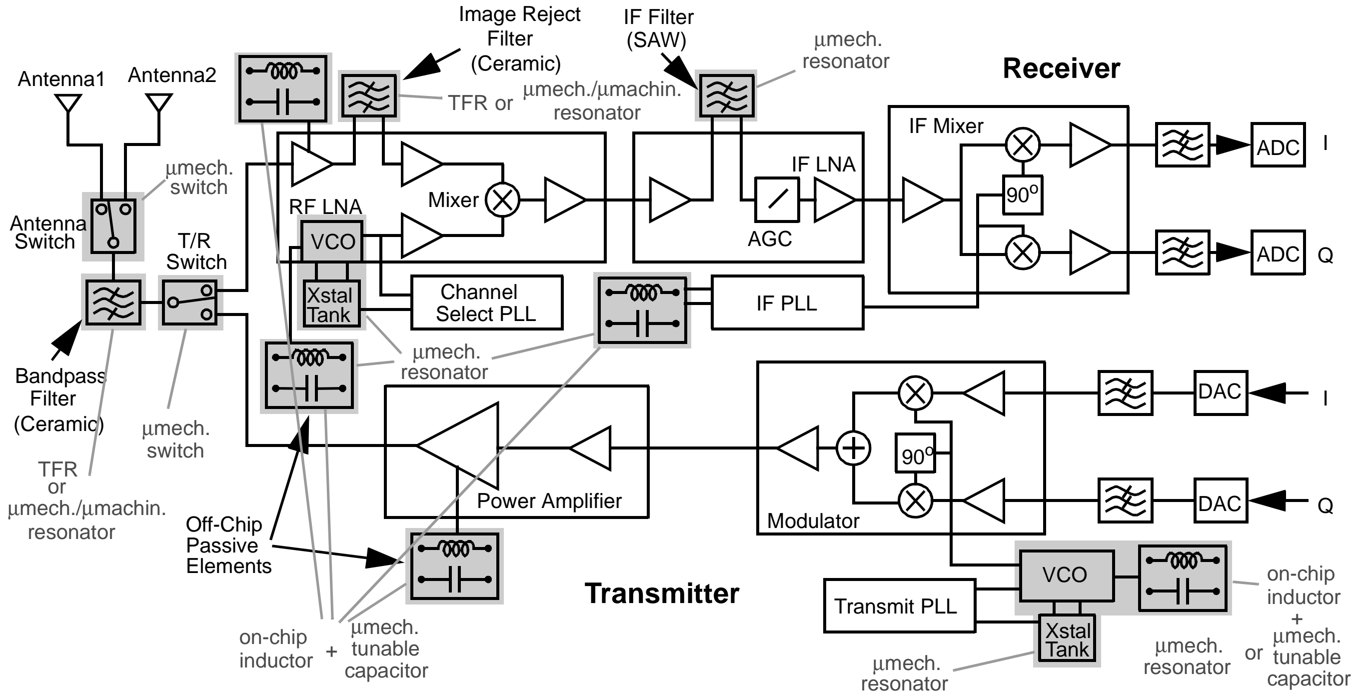

Fig. 1. System-level schematic detailing the front-end design for a typical wireless transceiver. The off-chip, high-Q, passive components targeted for replacement via micromechanical versions (suggestions in lighter ink) are indicated in the figure

single-crystal silicon and metallic technologies that not only offer solutions to these problems, but also enable other applications, including microwave and mm-wave filters, high-Q inductors, tunable capacitors, micromechanical switches, and temperature-desensitized vibrating mechanical resonators. Integration with electronics and encapsulation of devices for enhanced performance and stability are then covered in Sections 6 and 7, respectively. The paper concludes with brief comments on the potentially wide range of future communications applications addressable by micromachining.

Before considering the needed technologies, however, some understanding of the requirements of the devices they realize is necessary. Micromechanical filters are initially singled out for this purpose, since their design encompasses technology issues common to the majority of RF MEMS devices. Other applications are then considered as additional technologies are introduced.

2. MICROMECHANICAL FILTERS—A BRIEF OVERVIEW

Figures 2(a) and (b) show the perspective-view schematic, scanning electron micrograph (SEM), and measured frequency characteristic for a two-resonator very high frequency (VHF) bandpass micromechanical (abbreviated "µmechanical") filter.[3] As shown, this filter is comprised of two (often identical) clamped-clamped beam µmechanical resonators coupled by a flexural-mode beam. Ports for input v_i, output v_o, and frequency control $V_{\Delta f}$ signals are also provided, as are the necessary drive and sense circuitry. The operation of the above filter can be briefly summarized as follows:

(1) An electrical input signal is applied to the input port and converted to an input force by the electromechanical transducer (which for the case of Fig. 2(a) is capacitive) that can then induce mechanical vibration in x direction;

(2) mechanical vibration comprises a mechanical signal that is processed in the mechanical domain—specifically, the signal is rejected if outside the passband of the filter, and passed if within the passband; and

(3) the mechanically processed signal appears as motion of the output resonator and is re-converted to electrical energy at the output transducer, ready for processing by subsequent transceiver stages.

To fully understand the technological trade-offs under consideration when realizing a µmechanical filter, some understanding of filter modelling is required. The equivalent electrical circuit for the filter of Fig. 2(a) obtained via electromechanical analogy is shown in Fig. 2(c), where the constituent mechanical resonators are seen to correspond to LCR tank circuits, while the coupling beams are modeled via capacitive T-networks.[4] (The latter is expected when one considers that the coupling beams are actually acoustic transmission lines.[4]) Transformers are used to model electromechanical and purely mechanical

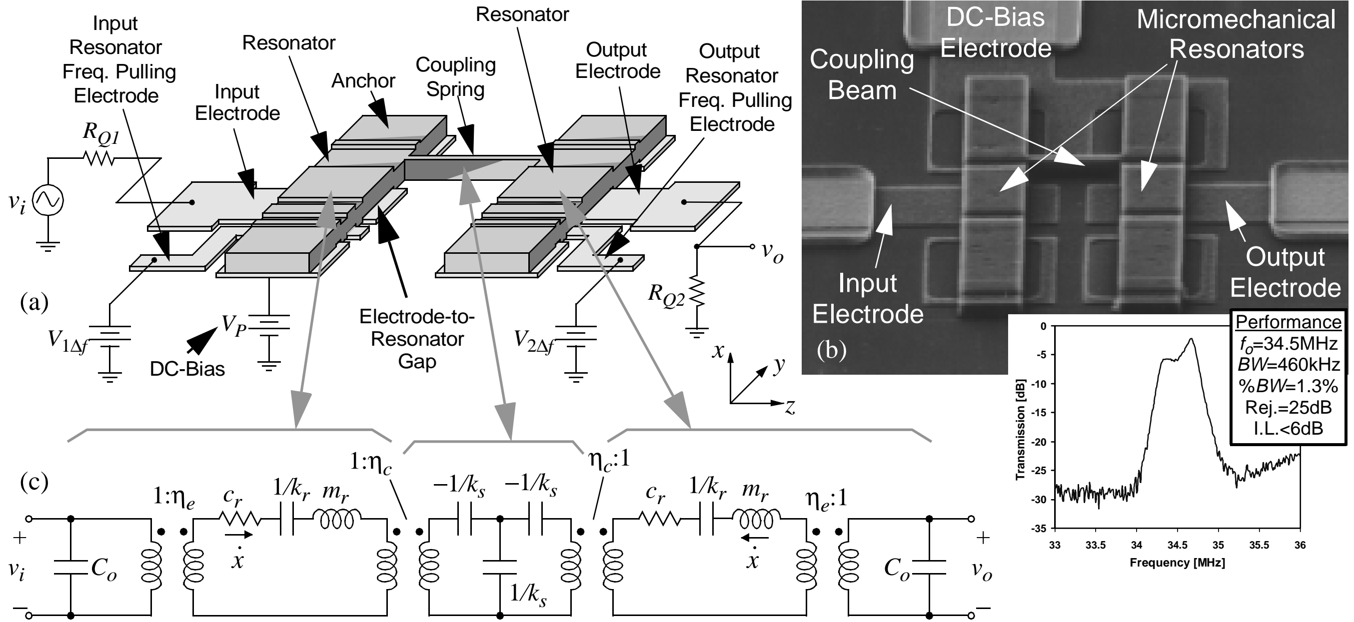

Fig. 2. (a) Perspective-view schematic of a two-resonator VHF μmechanical filter with typical bias, excitation, and signal conditioning electronics. (b) SEM of a VHF filter with measured frequency characteristic. (c) Electrical equivalent circuit for the filter in (a).

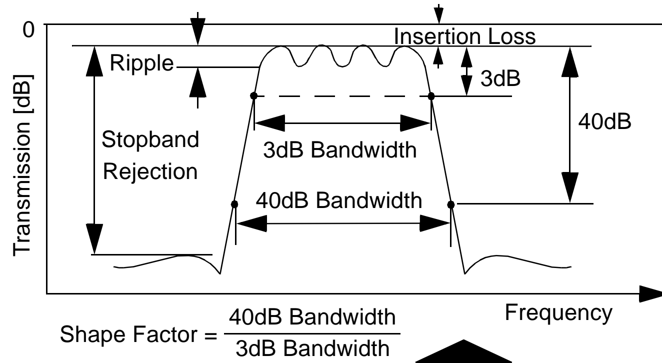

Fig. 3. Parameters typically used for filter specification.

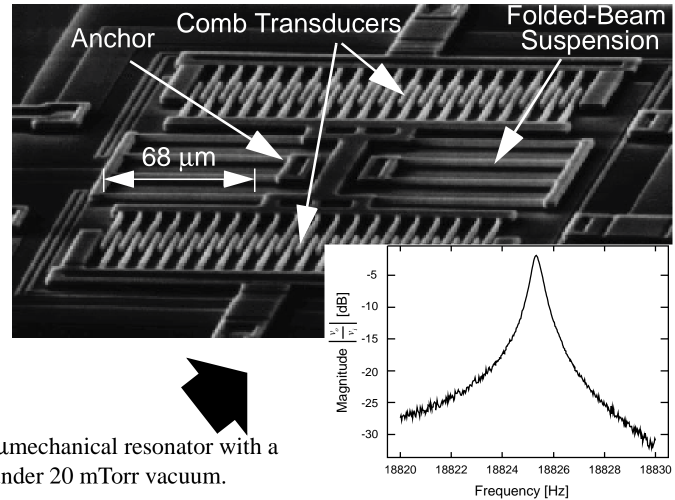

Fig. 4. SEM of an 18.8kHz folded-beam μmechanical resonator with a transmission spectrum measured under 20 mTorr vacuum.

impedance transformations[5] at the input/output ports and coupling locations, respectively. Filter designers will readily recognize the overall circuit topology in Fig. 2(c) to correspond to that for a coupled-resonator bandpass filter.

The series motional resistance R_x of the resonators seen at the input/output electrodes is of particular importance, since it determines the value of termination impedance R_Q required for proper filter operation. From the circuit of Fig. 2(c), R_x is the same for both resonators (since they are identical with identical port geometries) and can be expressed as[4]

$$R_x = \frac{\omega_o m_r}{Q\eta_e} = \frac{d^4\sqrt{k_r m_r}}{QV_P^2(\varepsilon_o A_o)^2}, \tag{1}$$

where Q is the resonator quality factor, ω_o is the radian center frequency, m_r and k_r are the resonator's effective mass and stiffness, respectively, at the electrode location, d and A_o are the electrode-to-resonator gap spacing and overlap area, respectively, ε_o is the free space permittivity, and V_P is the dc voltage across the electrode-to-resonator gap.

The performance of a bandpass filter is often quantified in terms of several parameters: insertion loss (which must be minimized); shape factor (again, minimized); and stopband rejection (maximize). These are all indicated pictorially in Fig. 3, which presents a typical bandpass filter specification. Insertion loss can be minimized for a given filter by using resonators with Q's much greater (e.g., >10×) than the Q_{fltr} of the filter. ($Q_{fltr}=f_o/BW$, where f_o is the filter center frequency, and BW is its

bandwidth.) Shape factor improves as the number of resonators in a given filter increases. However, unless the Q of the constituent resonators is sufficiently high, the number of resonators can be increased only at the expense of increased insertion loss. Thus, high resonator Q is also required for small shape factor. Finally, stopband rejection is dictated by not only shape factor, but also by the amount of parasitic feedthrough coupling the filter input to its output, which in turn is strongly dependent on the technology (e.g., whether sufficient grounding is available, or whether a shielding cap is available).

Another key design parameter that often is not a major consideration for off-chip filters, but that is of utmost importance for μmechanical filters, is termination impedance R_Q. In particular, a filter is normally designed to function correctly (i.e., with the desired passband shape) only when a specific value of impedance loads its input and output ports. For many systems, termination impedances around 50 or 75Ω (dictated by the antenna) are often required at RF, while larger values approaching 1-3kΩ are acceptable at IF frequencies. These impedances can be achieved by micro-scale filters only if sufficient electromechanical coupling is provided via the filter input and output transducers. The expression governing the termination resistance required for the filter of Fig. 2 depends upon R_x and can be expressed as[4]

$$R_Q = R_x\left(\frac{Q}{q_i Q_{fltr}} - 1\right) \propto \frac{d^4}{V_P^2 A_o^2}, \tag{2}$$

where Q_{fltr} is the filter quality factor, q_i is a normalized coefficient obtained from a filter cookbook,[6] and where the most practical controllable parameters have been singled out in the final expression to the far right. As dictated by (2), R_Q is strongly dependent on the dc-bias V_P applied across the port in question and on the electrode-to-resonator gap spacing d. In many of today's portable wireless applications, the supply voltage is greatly limited, so increasing V_P may not be an option. Overlap area A_o may also be constrained by resonator geometry. The gap spacing d, on the other hand, is limited mainly by technology. To achieve termination impedance values on the order of 50Ω for VHF to UHF filters, gap spacings of less than 500Å are required (the exact value depending heavily on $\%BW$ and V_P). For termination resistances greater than 1kΩ, gap spacings greater than 1000Å can be utilized.

3. POLYSILICON SURFACE MICROMACHINING

Polycrystalline silicon has so far been the material of choice for HF and VHF vibrating μmechanical resonators intended for bandpass filters and stable reference oscillators. The reason is that polysilicon offers an excellent compromise between high material Q and maximum design flexibility. In particular, the Q of polysilicon μmechanical resonators under vacuum has been measured in excess of 50,000 at MF frequencies (Fig. 4)[7] and on the order of 10,000 at VHF frequencies (Fig. 5). (Note that vacuum is necessary to attain these Q's, since at atmospheric pressure these micro-scale resonators must expend a significant fraction of their total energy per cycle to push air molecules aside.[8]) In addition, geometric design flexibility is especially important when implementing complex filters, such as the MF three-resonator version shown in Fig. 6, which features numerous additional ports for feedthrough suppression and post-fabrication tuning.[9] For devices as complex as this one, polysilicon surface micromachining—in which critical features are defined in a single masking step (no alignment necessary) and anchors can be placed virtually anywhere on the substrate surface—constitutes one of the best technological choices.

The fundamental procedure behind polysilicon surface micromachining[10] is summarized succinctly in Fig. 7. In this procedure, a sequence of IC-compatible film depositions and patternings are used to achieve a structure with the cross section shown in Fig. 7(a). Here, after definition of isolation dielectrics and polysilicon interconnect, a (sacrificial) oxide layer is temporarily used to support the structural polysilicon layer during deposition, doping, and patterning. After achieving the structure of Fig. 7(a), the whole structure is immersed in a solution of hydrofluoric acid (HF), which attacks the sacrificial oxide layer, but leaves the polysilicon layer relatively intact. The result: A free standing polysilicon beam, free to move in any direction upon application of an electrostatic force. It should be mentioned that Fig. 7 omits many important details that must be considered in actual fabrication runs. In particular, the intrinsic Q of resulting resonators has been found to be heavily dependent upon several process details, including the method used to dope the polysilicon material.[4] Post-process steps, such as localized annealing, can also greatly influence resonator Q and stability.[11]

Figure 7 actually illustrates a very conventional polysilicon surface micromachining process, used frequently for commercial products[12] and used for the MF filter of Fig. 6 (and for the MF oscillator of Fig. 25(b)). This process is fairly conservative in that 2 μm sacrificial oxide spacers are utilized. Thus, high frequency capacitively-transduced filters using resonators moving perpendicular to the substrate cannot use this process for reasons discussed in the previous section: gaps on the order of from 200Å to 1000Å are required between electrodes and polysilicon structures. Lithographically, submicron lateral gaps for resonance parallel to the substrate are possible via e-beam lithography combined with aggressive etch technologies (discussed later), but this approach still requires extensive research. Thus, although many MF resonators have benefited from the flexibility of lateral vibration (Fig. 6), lithographic limitations have so far prevented practical VHF μmechanical resonators and their

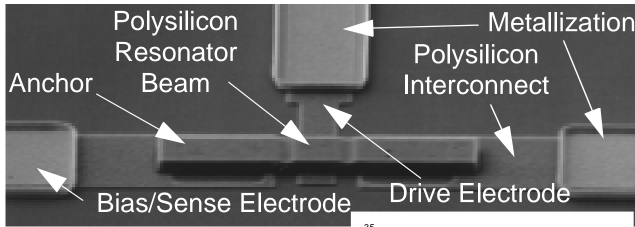

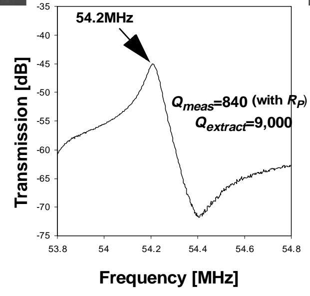

Fig. 5. SEM of a 54.2 MHz folded-beam micromechanical resonator with a transmission spectrum measured under 20 mTorr vacuum.

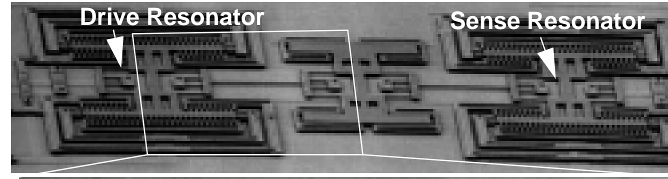

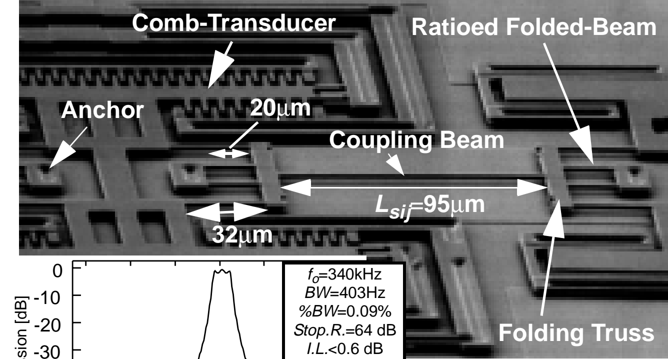

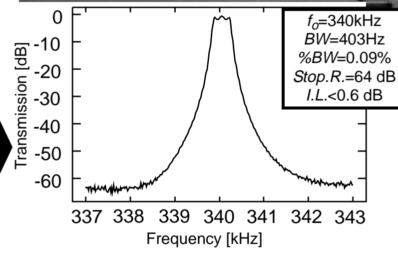

Fig. 6. Full-view (a) and zoom-in (b) SEM's of a three-resonator, MF, micromechanical filter with measured transmission spectrum.[5] This filter features ratioed folded-beam, comb-driven resonators that vibrate parallel to the substrate.

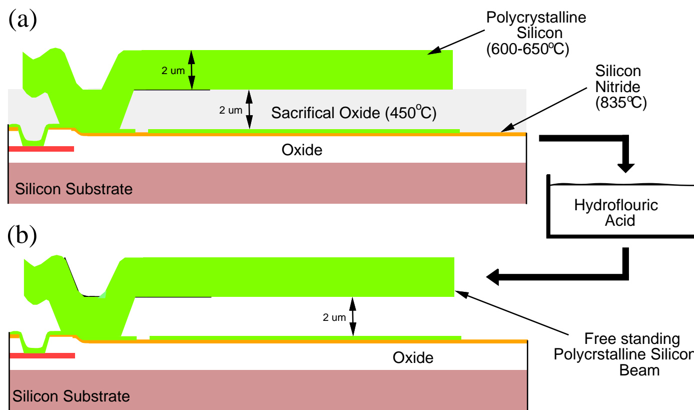

Fig. 7. Cross-sections depicting the fabrication sequence used in polysilicon surface micromachining. (a) Required film layers up to the release etch step. (b) Resulting free-standing beam following a release etch in hydrofluoric acid.

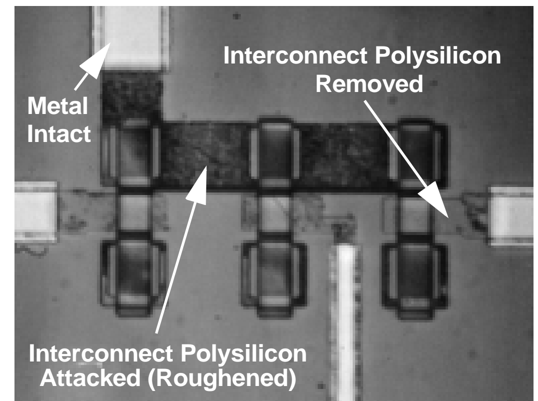

Fig. 8. Overhead-view photograph showing compromised polysilicon, but intact chrome/gold metal, in the electrodes after a 30 minute sacrificial release step in hydrofluoric acid.

associated filters from vibrating parallel to the substrate. Rather, these devices vibrate perpendicular to the substrate, with electrode-to-resonator gaps defined by sacrificial oxide thicknesses, which can easily be made down to 200Å or less. In particular, the 54.2 MHz polysilicon μmechanical resonator of Fig. 5 features a 300Å electrode-to-resonator gap.

Unfortunately, the use of such a small vertical gap in polysilicon surface micromachining comes riddled with several processing details/hindrances. Many of these arise from the now very thin sacrificial oxide layers used to define these gaps, and can be enumerated as follows:

(1) Sacrificial layer uniformity is now an issue, and precautions must be taken to prevent pinholes.

(2) In previous large-spacer surface micromachining processes, the sacrificial oxide protected underlying interconnect polysilicon layers during the overetch step in structural polysilicon patterning. For the case of thin gaps, however, the sacrificial oxide may no longer be thick enough to protect underlying layers when conventional RIE etchers are used. Rather, high density plasma etchers with much higher silicon-to-oxide etch selectivities may now be required.

(3) Due to reactant diffusion limitations, the sacrificial etch takes much longer with thin gaps than for previous large-gapped processes. This is problematic, because although HF attacks polysilicon much more slowly than

oxide, it still attacks at a finite rate. Attack of polysilicon interconnect by HF has been observed, as has evidence of dopant extraction from polysilicon by HF during long release etches, both of which greatly increase the series resistance of resonator input and output electrodes.

The increase in series resistance described in item (3) is quite detrimental to resonator performance, and is largely responsible for the low value of *measured* Q shown in Fig. 5. For cases where polysilicon alone (i.e., no metallization) is used as interconnect, the phenomena in item (3) can lead to electrode R_S's (both input and dc-bias electrodes) on the order of from 2-10kΩ for the resonator of Fig. 5, depending upon the needed release etch time. With metallization, where all polysilicon interconnect is covered by metal except for those portions within 15 μm of the resonator, R_S can be reduced to 0.15-2kΩ. For the particular resonator of Fig. 5, the total on-chip interconnect resistance amounted to ~180Ω, which, considering a calculated value for R_x=28Ω for this resonator (under the measurement conditions used for Fig. 5), can still seriously load the Q of the resonator. Thus, the measured Q in the spectrum of Fig. 5 actually represents the loaded Q (Q_{loaded}), not the actual resonator Q. The loaded Q is given by the expression

$$Q_{loaded} = Q\left(\frac{R_x}{R_x + R_S}\right), \tag{3}$$

which stresses the importance of minimizing R_S relative to R_x. Rearranging (3), the actual unloaded Q of the resonator is found to be about 9,000. Thus, the Q of this resonator has been severely degraded from 9,000 to 840 by the excessive parasitic series resistance. To illustrate the severity of such Q-degradation: A 70 MHz, 0.3% bandwidth, three-resonator filter implemented using resonators with Q's of 9,000 would show an insertion loss of ~1.5dB—very good. In contrast, if resonators with Q's of 840 were used, the insertion loss would be ~20dB, which is unacceptable for most applications.

The Q of the resonator of Fig. *5* could be maximized if the electrodes were comprised entirely of metal. Unfortunately, many fabrication sites (including ours) cannot do this, due to a need to keep metal contamination away from polysilicon and oxide LPCVD tubes used for circuits processes, as well as micromechanics. Thus, the metal/poly composite interconnect of Fig. *5* was merely a good compromise. At first glance, metallization seems straightforward via a simple lift-off technique. However, the long HF release etch required for small gaps, combined with electrolytic reactions, greatly complicate the metallization process. In particular, the type of metal used must be carefully selected to insure a sufficiently low rate of attack by HF. Although aluminum etches very slowly in 48.8 wt. % concentrated HF, the etch rate is not slow enough to withstand a very long, small-gapped, release etch. Chrome/gold metallization is a better choice for HF release etches. Unfortunately, however, chrome/gold in contact with polysilicon in an HF solution gives rise to an electrolytically enhanced reaction that dissolves away the polysilicon layer. The end result is shown in Fig. 8, where obvious removal of polysilicon interconnect is seen, while the metal remains intact. The resulting polysilicon shows R_S's as high as 50kΩ—quite unacceptable for high Q applications.

The solution to the above problem is to metallize *after* the release etch. For this to be practical, the released structures must be able to withstand a photoresist spin cycle. This is not a problem for high frequency μmechanical resonators, which have stiffnesses on the order of 2,000 to 100,000 N/m, but can be a problem for very compliant structures, such as those used for accelerometers, which have stiffnesses on the order of 1 N/m or less. Also worth mentioning for post release metallization is the need to keep the metal defining photoresist on the wafer during dicing, so that the dicing slurry does not interfere with the resonators, e.g., by seeping into gaps and/or contaminating the resonator surfaces.

Although metallization helps to greatly reduce interconnect series resistance, it may not be enough in many cases, since the metal cannot cover the polysilicon interconnect near the resonator. If buying extra LPCVD tubes that allow metal electrodes is not an option, other strategies that reduce the resistance in polysilicon interconnect are needed.

One strategy presently under investigation attempts to return to lateral resonator operation, as illustrated in Fig. 9, where vibrations parallel to the substrate are now excited by lateral gap capacitive transducers. Here, much thicker electrodes can be used, resulting in much smaller polysilicon electrode R_S's, on the order of 1-2Ω. Also, the dopant loss and interconnect attack problems described above are no longer factors. The cross-section of Fig. 9 can be achieved in a surface-micromachining process using e-beam lithography and high density plasma etching to define resonator and electrode features. Fig. 10 shows work towards the structure of Fig. 9, in which an inductively coupled (ICP) high density plasma source is used with a nickel mask to dry etch 0.1 μm gaps in 3.1 μm-thick silicon using a Cl_2 chemistry.[13] Although promising, this technique presently cannot match the d's and A_o's of vertical resonator processes. In particular, as dictated by (3), until sub-500Å gaps can be achieved in polysilicon films thicker than 5 μm, lateral resonator technologies such as this will struggle to achieve filters with termination resistance values less than 100Ω. In the meantime, other technologies have recently arisen that may allow thin lateral gaps between much thicker silicon layers. One very recent technology uses conformal carbonated parylene to achieve vertical sacrificial layers for more accurate molding in hexsil processes.[14] Sacrificial layer removal is done using an oxygen plasma, which

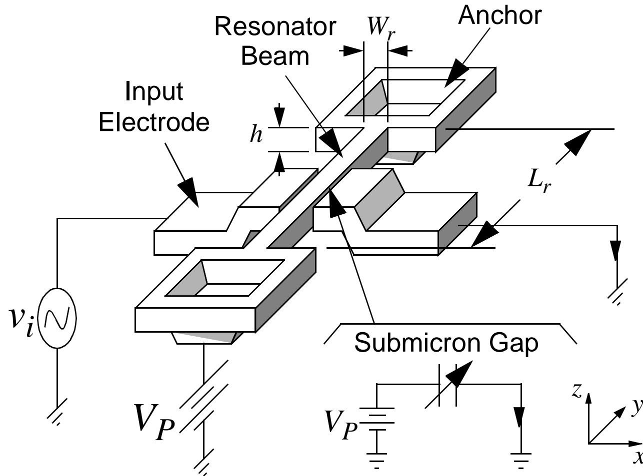

Fig. 9. Small-gapped lateral μmechanical resonator design that reduces electrode series resistance.

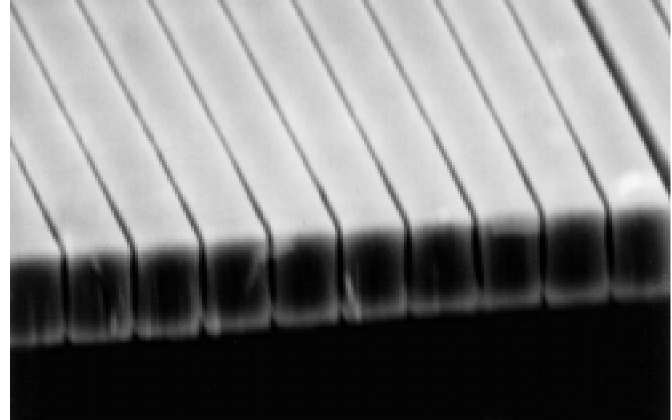

Fig. 10. SEM of 3μm-thick silicon fingers separated by 0.1μm gaps attained using a Cl_2-based high density ICP plasma etch.[13]

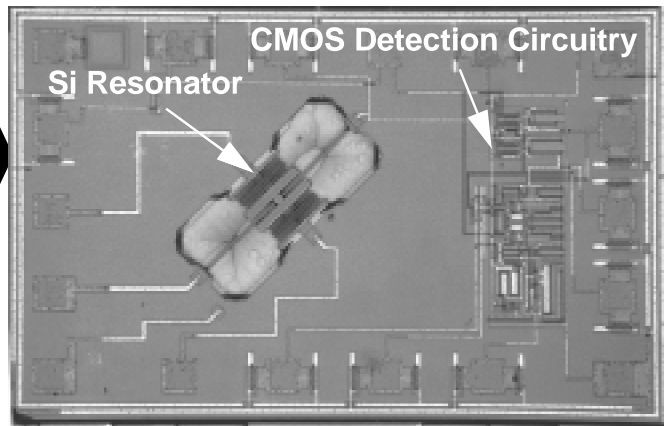

Fig. 11. Overhead-view of a single-crystal silicon lateral micromechanical resonator merged with sense electronics in a single planar process.[18]

prevents attack of structural layers. This technology has good potential for application to surface-micromachining.

Thus far, this discussion has centered on polysilicon μmechanical resonators utilizing capacitive transduction. This emphasis reflects the fact that virtually all successful μmechanical filters (using two resonators or more) to date have utilized capacitive transduction. This statement in turn reflects the advantages of capacitive transduction, which include process simplicity and less susceptibility to bimorph-derived temperature dependencies. Nevertheless, capacitive transduction does have its drawbacks. In particular, its electromechanical coupling coefficient depends inversely on the electrode-to-resonator overlap area A_o. Thus, with capacitive transduction, increasing resonator frequency to satisfy higher communication bands is no longer just a matter of reducing resonator geometries; rather, alternative designs that attain higher frequencies without excessive reductions in A_o must be used. On the other hand, such alternative resonator designs may be avoidable via alternative transduction techniques, such as piezoelectric[15] and magnetomotive.[16] These methods, however, also have drawbacks. In particular, piezoelectric materials are difficult to deposit uniformly, and piezoelectric transduction often entails the use of bilayer structures with potentially increased temperature sensitivity. For the case of magnetomotive transduction, the permeabilities of the magnets used have limited bandwidths and are thus not effective at UHF frequencies. The search for optimum transduction methods continues.

4. SINGLE-CRYSTAL SILICON BULK MICROMACHINING

For some communications applications, even higher Q's than attainable via polysilicon resonators may be required. For example, the reference oscillators for satellite communications and for Doppler radar must be ultra-stable, with typical phase noise requirements around −150dBc/Hz at a 67kHz carrier offsets for Doppler radar.[17] To attain this degree of short-term stability, resonators with extremely high Q's are required. Although polysilicon has shown Q's up to 10^5 at MF frequencies, it has yet to show comparable Q's at VHF, where measured Q's have been in the tens of thousands. Single-crystal silicon, on the other hand, with fewer loss-generating defects than its polycrystalline counterpart, has posted Q's in excess of 10^6 at MF. Provided these remain comparatively high at VHF, this material should be a good candidate for ultra-stable applications.

A μmechanical resonator fabricated in single-crystal silicon using a technology that allows integration with transistor circuits is shown in Fig. 11.[18] The associated process flow is shown in Fig. 12. In both figures, the most important restriction of the majority of bulk micromachining processes is clearly illustrated: Anchors cannot be placed arbitrarily, as is possible in a surface micromachining process; rather, unless a much more complex process is used, they must be realized as attachments to silicon sidewalls. This greatly restricts the variety of μmechanical resonator designs possible. In particular, it precludes the use

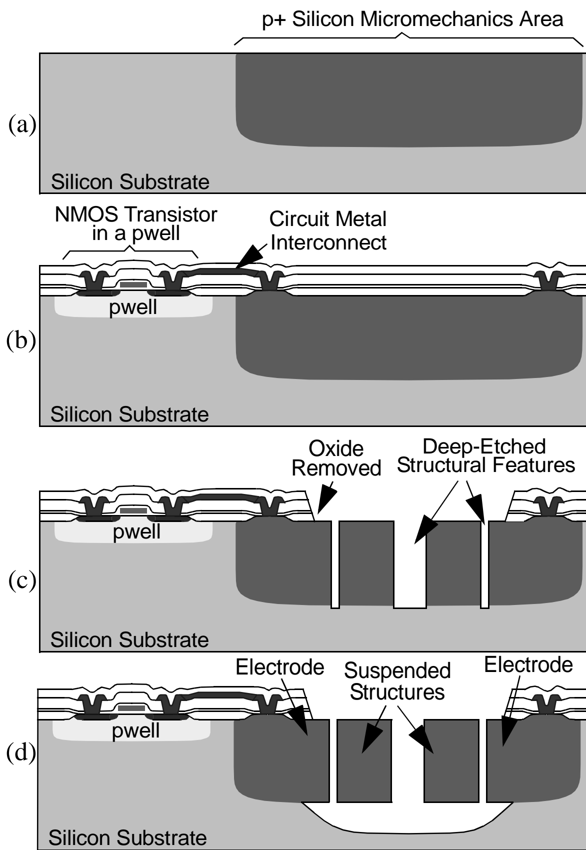

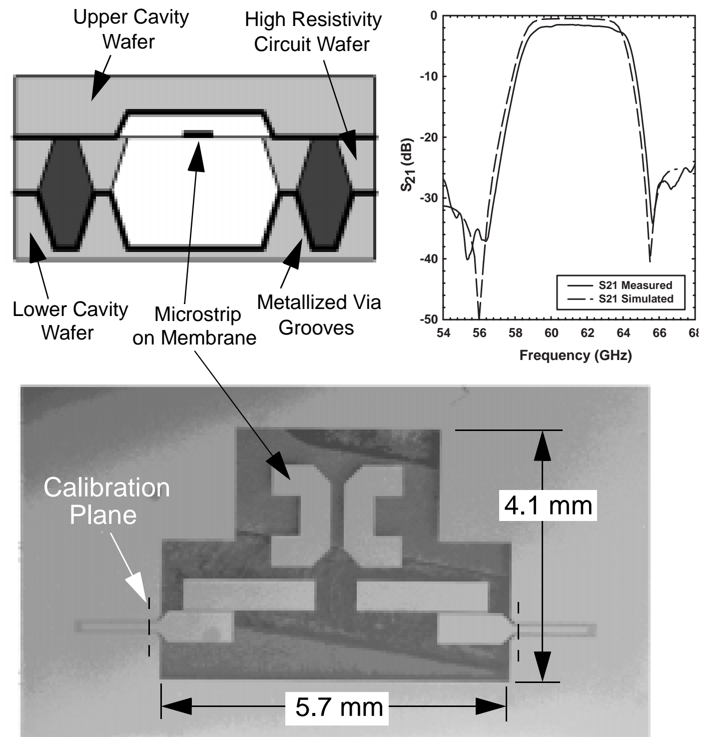

Fig. 13.A 60 GHz 8% bandwidth 4-pole micromachined elliptic filter with a resonator width of 500 μm, a resonator Q of 500, and an insertion loss of 1.5 dB.[20]

Fig. 12.Process flow for the merged single-crystal silicon micromechanics/CMOS process of Fig. 11.[18] (a) Define the p+ silicon micromechanical material via boron diffusion. (b) Run a conventional circuits process. (c) ICP high density plasma etch through the p+ region and into the silicon wafer. (d) EDP release etch.

of folded-beam structures, which, as will be seen, could be the key to attaining improved temperature stability—another important quality for oscillator frequency references. In effect, although single-crystal silicon technologies have the potential to enhance short-term stability in oscillators via higher Q's, these enhancements may be at the expense of long-term stability (i.e., thermal stability) if single-crystal silicon processes continue to be relatively inflexible.

Vibrating μmechanical resonators are certainly not the only communications devices achievable via bulk micromachining. EDP- and KOH-based bulk micromachining approaches[19] have recently been used to isolate microwave and mm-wave waveguide resonators from substrate parasitics and adjacent interferers, greatly reducing losses. Figure 13 shows a 60 GHz 8% bandwidth 4-pole micromachined elliptic filter with a resonator width of 500 μm and a resonator Q of 500. The insertion loss in the passband is 1.5 dB referenced to the calibration planes. In addition, due to the fully enclosed package (achieved via bulk micromachining and bonding), the typical measured isolation between adjacent transmission lines is -50dB at 30 GHz, and −45 dB between closely spaced filter banks at 10 GHz.[20] Bulk micromachined membrane technologies have also been used to realize more efficient dipole and slot antennas that effectively radiate in free space when suspended on thin membranes. Anisotropic etching has also been used to integrate silicon pyramidal cavities that act as miniature integrated horns around the dipole antennas, directing the radiated energy very efficiently in the forward direction.[21] Finally, synthesized artificial dielectric-constant substrate materials have been achieved by etching carefully placed via holes in the dielectrics under antennas, greatly increasing antenna efficiencies at microwave frequencies.[22]

5. METAL MICROMACHINING

The first μmechanical resonators were actually fabricated in the mid 1960's in electroplated gold metal using a process similar to the surface-micromachining process described by Fig.7.[24] Unfortunately, these earlier metal processes were plagued with aging problems and exhibited Q's on the order of only 90, so were not useful for many IF filtering and oscillator applications. These problems, along with surface charge problems associated with exposed gate sensing structures, ended research efforts in this area shortly after 1967.

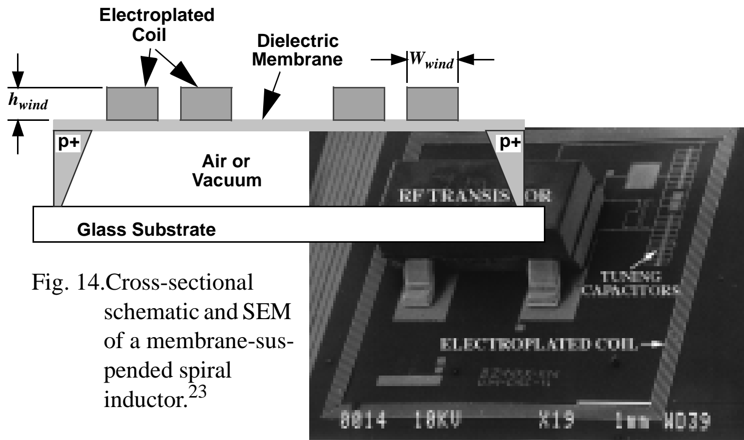

Fig. 14.Cross-sectional schematic and SEM of a membrane-suspended spiral inductor.[23]

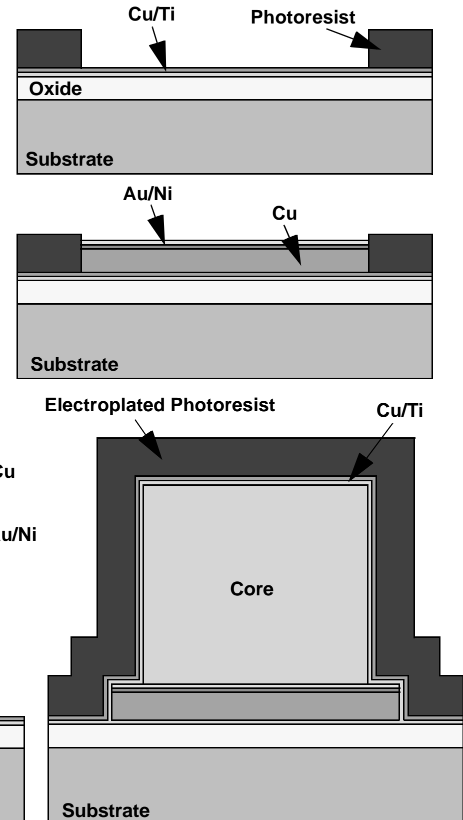

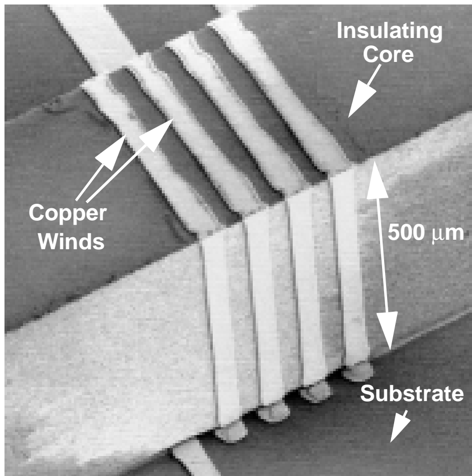

Fig. 15.SEM of a three-dimensional micromachined coil inductor.[25]

Fig. 16.Process flow for the inductor of Fig. 15.[25] (a) Oxide and Cu/Ti seed layer deposition and photoresist patterning. (b) Cu plating and Au/Ni passivation. (c) Alumina core attachment, Cu/Ti seed layer deposition, photoresist plating. (d) Pattern photoresist via direct-write 3D lithography, plate Cu, deposit Au/Ni passivation, remove photoresist.

Although not a first choice for vibrating resonator applications, metal technologies have certainly been important for other communications applications. In particular, the Q of integrated inductors and tunable capacitors, and the insertion loss of µmechanical switches, are all heavily dependent upon the series resistance of their construction materials. Thus, metals have been a natural material choice for these applications.

For the specific case of inductors comprised of metal spirals or coils, series resistance in the turns, losses to the surroundings (i.e., to the substrate), and parasitic capacitance coupling the turns to each other and to the substrate, must all be minimized. The reasons: (1) Series resistance and other losses degrade the inductor Q, and (2) Parasitic capacitance can resonate with the inductor itself, giving rise to a self-resonance that limits the operating frequency of this inductor. To attain lower series resistance, thicker metal lines can be achieved via electroplating technologies. To reduce substrate couplings, bulk micromachining techniques based on EDP, KOH, or TMAH chemistries[19] can be used to remove the substrate in similar fashion to the microwave filter of Fig. 13. Figure 14 presents the cross-sectional schematic and SEM of an inductor realized using these two strategies to maximize the QL product. This inductor has a value of 115nH and exhibits a Q of 22 at 275 MHz with a self-resonance frequency of 750 MHz.[23] Inductors at microwave frequencies have also been realized using these strategies, achieving inductances on the order of 1.2 nH with associated self-resonance frequencies of 70 GHz with substrate removal, and 22 GHz without substrate removal, with expected Q's of 60-80 at 40 GHz.

An alternative method for inductor construction has recently emerged in which electroplated photoresist combined with an exotic three-dimensional lithographic technology are used to achieve the coil inductor shown in Fig. 15.[25] Fig. 16 summarizes the process flow for this inductor. This coil inductor can outperform its spiral counterparts in both Q and self-resonance frequency, because its coupling region is better isolated from the substrate, and metal turns can be made wider to reduce series resistance with less capacitance increase and less reduction in inductance value. The device of Fig. 15 achieves and induction of 4.8nH with a Q of 30 at 1 GHz, and a self-resonance frequency of 4 GHz—some of the best values to date for a 1 GHz, on-chip inductor.

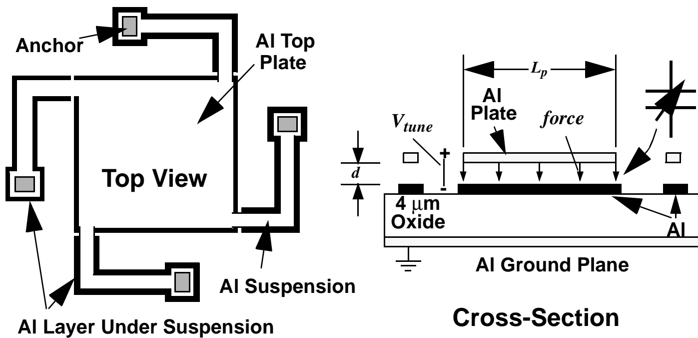

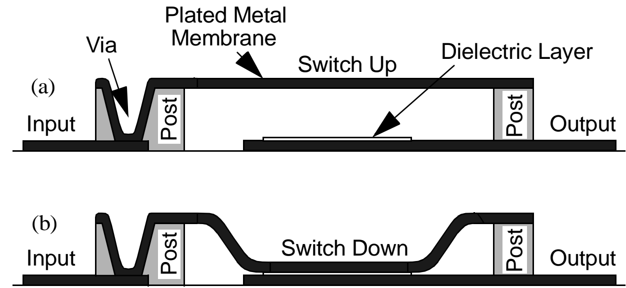

Fig. 18.Cross-sectional schematics of a typical micromechanical switch: (a) Switch up. (b) Switch down.[27]

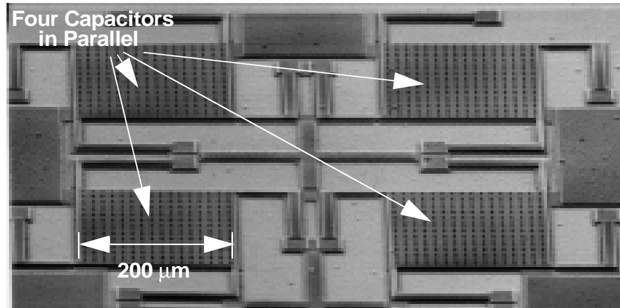

Fig. 17.Schematics and SEM of a surface-micromachined, aluminum, voltage-tunable capacitor.[26]

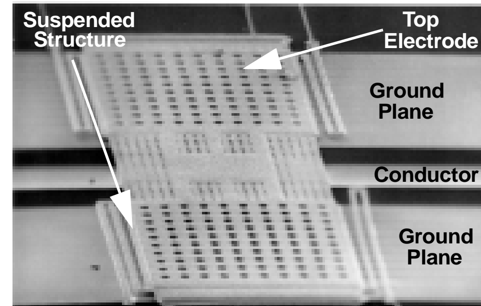

Fig. 19.Micromechanical switch designed for faster, lower voltage operation and higher power handling capability.[28]

In most practical applications, inductors must be combined with low loss capacitors. For example, integrated voltage-controlled oscillators (VCO's) require not only miniaturized inductors, but *tunable* high-Q capacitors, as well. Previous attempts to use reverse-biased diode junction capacitors as tunable on-chip capacitors have been foiled by excessive series resistance in these silicon devices, which greatly degrades their Q's. Here again, metal micromechanical technology provides a solution in the form of the tunable, metallic, parallel-plate capacitor shown in Fig. 17.[26] For this device, surface-micromachining (similar to that of Fig. 18) is used to suspend a top aluminum plate above a bottom one via flexural supports. The distance (i.e., capacitance) between the two plates can then be varied electrostatically by adjusting a voltage V_{tune} between them. The capacitor in the SEM of Fig. 17 uses four such plates in parallel to achieve a total capacitance of 2.2pF with an overall Q of 60 (limited by series resistance in the supports), and tunable over 16% with a 5.5V change in V_{tune}.

Yet another RF application of metal micromachining technology is that of micromechanical switches. These devices are similar in form to the capacitor of Fig. 17, except they are operated in a binary (as opposed to analog) mode, where input voltages are applied such that the top plate is either fully up or down. Because only two-states are important for switches, the majority of them have used fairly simple air-bridge or membrane designs, such as shown in Fig. 18.[27] For such switches, the important performance metrics are the on- and off-state impedances (minimize and maximize, respectively), the required actuation voltage (minimize), and the switching time (minimize). Micromechanical switches consume much less power and exhibit much lower insertion loss than their active diode or transistor counterparts, and can be made highly linear, with extrapolated IP3 points up to 66 dBm.[1] These characteristics make them very useful as phase shifters for phased array antennas, as well as in transmit/receive junctions and configurable filters, where they switch capacitor values around. Most switches are manufactured using surface-micromachined deposited or plated metal processes. To date, application of micromechanical switches has been encumbered by a need for large actuation voltages (~20-30V) and by slower switching times (~1−10μs) than active counterparts. A new switch design (Fig. 19), however, has recently been introduced that uses serpentine suspensions and large actuation plates for faster operation with lower actuation voltages, as well upper electrode plates for off-state stability and higher power handling capability.[28]

Finally, although reasons why metals may not be the optimum technology for vibrating μmechanical resonators were given at the beginning of this section, there is still active research aimed at using metal technologies to implement high-Q resonators. These efforts exist due to several potential advantages of metal technologies over silicon, including lower interconnect series resistance, ease of merging with integrated circuit transistor electronics (c.f., Section 6), and the possibility of attaining temperature-insensitive resonators over silicon substrates. The last of these is achieved using geometric compensation techniques, in which resonator geometries are chosen such that temperature-induced stress variations in resonator stiffness counteract frequency changes due to Young's modulus temperature dependence.[11] The SEM for a simple folded-beam resona-

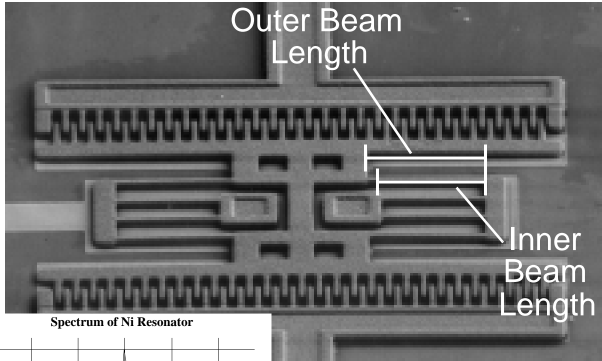

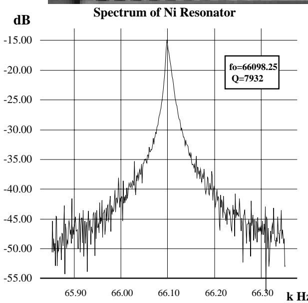

Fig. 20.SEM of a geometrically temperature-compensated ratioed folded-beam µmechanical resonator with measured frequency spectrum.[11]

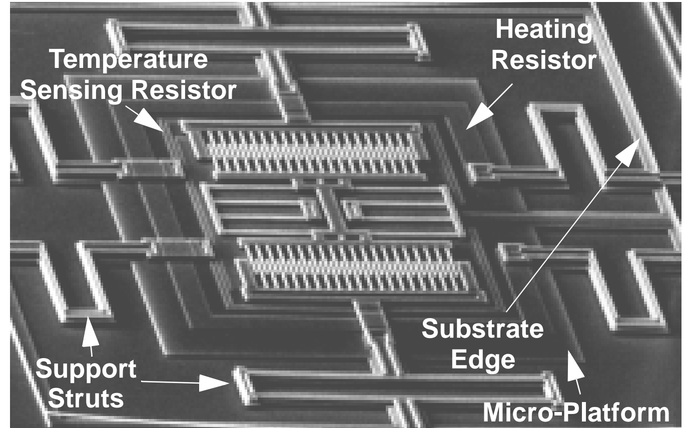

Fig. 22.SEM of a surface-micromachined micro-oven supporting a polysilicon µmechanical resonator.[29]

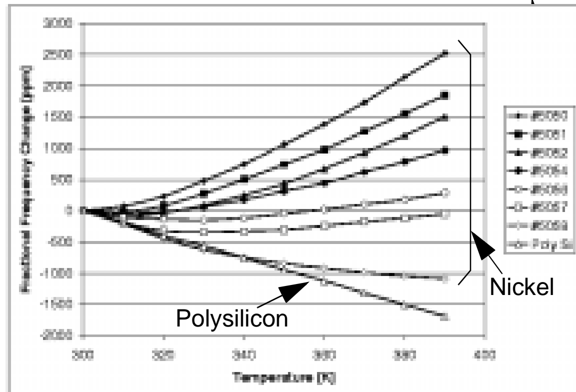

Fig. 21.Measured plot of normalized frequency vs. temperature for several Fig. 20 resonators with varying inner-to-outer folded-beam ratios.[11] The curve for an equal beam length polysilicon µresonator is also included for comparison.

tor design that achieves such geometric compensation is shown in Fig. 20. Here, the lengths of the inner and outer folded beams are made unequal so that under a temperature change one expands/ compresses at a different rate than the other, introducing stresses in both beams that vary with temperature. Note that such geometric compensation techniques are most effective if the resonator and substrate materials have different thermal expansion coefficients; i.e., this design doesn't work well for polysilicon resonators over silicon. Figure 21 shows measured plots of fractional frequency change versus temperature for nickel resonators with varying inner-to-outer folded beam length ratios. (The curve for an equal folded-beam polysilicon resonator is also included for reference.) Via appropriate ratioing, the total resonator temperature variation from 27°C to 117°C has been reduced from 1750 ppm for the equal beam, polysilicon case to 300 ppm for the 50/57 ratioed nickel resonator case. Perhaps more importantly, a valley in the fractional frequency versus temperature curve has been introduced, at which a low power micro-oven (Fig.22[29]) can be biased for maximum thermal stability. In addition, the Q of the µmechanical resonator in Fig. 20 is about 8,000, achieved using a slowed nickel plating process.[11] This is quite an improvement over the Q of 90 from 1967.[24] Research to achieve ultra-temperature stable oscillators using this technique is presently underway.

6. CIRCUITS/MICROMECHANICS INTEGRATION

To maximize the benefits of miniaturized micromachined communication devices, it is highly advantageous to minimize the capacitance incurred via interfacing with transceiver electronics. This would allow the use of higher impedances within the system, which would both lower the power consumption of many of the transistor functions (e.g., buffers coupling low noise amplifiers to filters) and would relax the technology requirements needed to achieve smaller termination impedances for µmechanical filters. In addition, an interfacing technology with the ability to support the use of large numbers of micromechanical components is desirable, since it allows the designer to capitalize on novel communication architectures that use massive arrays of filters to reduce desensitization in receivers while allowing much reduced power consumption.[30]

Several technologies that merge many of the aforementioned micromachining processes with those for integrated circuits have been developed and implemented over the past several years. These technologies can be categorized into three major approaches:

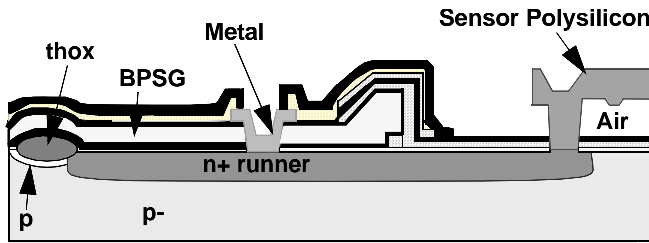

Fig. 23.Cross-section of the sensor area in Analog Devices' BiMOSII process.[12]

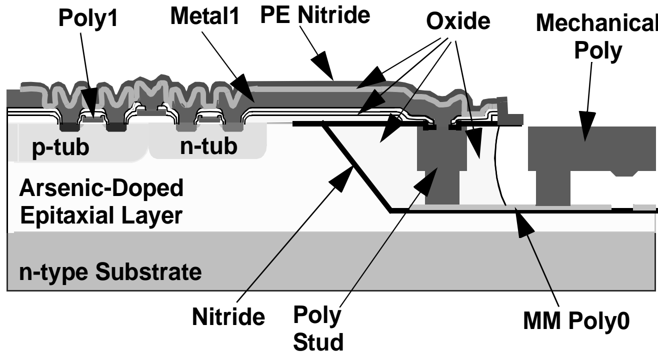

Fig. 24.Cross-section of Sandia's *iMEMS* process.[31]

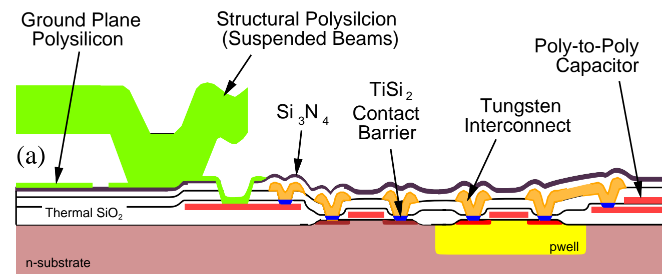

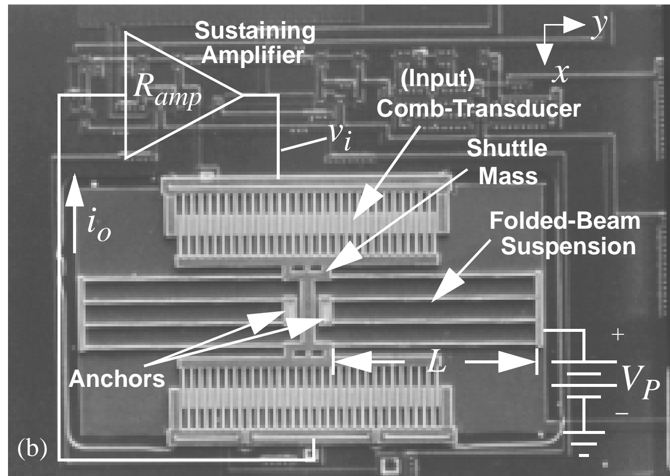

Fig. 25.(a) Cross-section of the MICS process.[32] (b) Overhead-view of a fully integrated micromechanical resonator oscillator fabricated using MICS.[33]

(1) *Mixed Circuit and Micromechanics*, in which steps from both the circuit and the micromachining processes are intermingled into a single flow. Of the three approaches, this one has so far seen the most use. However, it suffers from two major drawbacks: (i) many passivation layers are required (one needed virtually every time the process switches between circuits and micromechanics); and (ii) extensive re-design of the process is often necessary if one of the combined technologies changes (e.g., a more advanced circuit process is introduced). Analog Devices' BiMOSII process (Fig. 23[12]), which has successfully produced a variety of accelerometers in large volume, is among the most successful examples of mixed circuit/micromechanics processes.

(2) *Pre-Circuits*, in which micromechanics are fabricated in a first module, then circuits are fabricated in a subsequent module, and no process steps from either module are intermingled. This process has a distinct advantage over the mixed process above in that advances in each module can be accommodated by merely replacing the appropriate module. Thus, if a more advanced circuit process becomes available, the whole merging process need not be redesigned; rather, the circuits module need only be replaced. An additional advantage is that only one passivation step is required after the micromechanical module. One of the main technological hurdles in implementing this process is the large topography leftover by micromechanical processes, with features that can be as high as 9 µm, depending upon the number and geometry of structural layers. Such topographies can make photoresist spinning and patterning quite difficult, especially if submicron circuit features are desired. These problems, however, have been overcome by researchers at Sandia National Laboratories, whose *iMEMS* process (Fig. 24) performs the micromechanics module in a trench, then planarizes features using chemical mechanical polishing (CMP) before doing the circuits module.[31]

(3) *Post-Circuits*—the dual of pre-circuits—in which the circuits module comes first, followed by the micromechanics module, where again, no process steps from either module are interspersed. This process has all the advantages of pre-circuits, but with relaxed topography issues, since circuit topographies are generally much smaller than micromechanical ones. As a result, planarization is often not necessary before micromechanics processing. Post-circuit processes have the additional advantage in that they are more amenable to multi-facility processing, in which a very expensive fabrication facility (perhaps a foundry) is utilized for the circuits module, and relatively lower capital micromechanics processing is done in-house at the company site (perhaps a small start-up). Such an arrangement

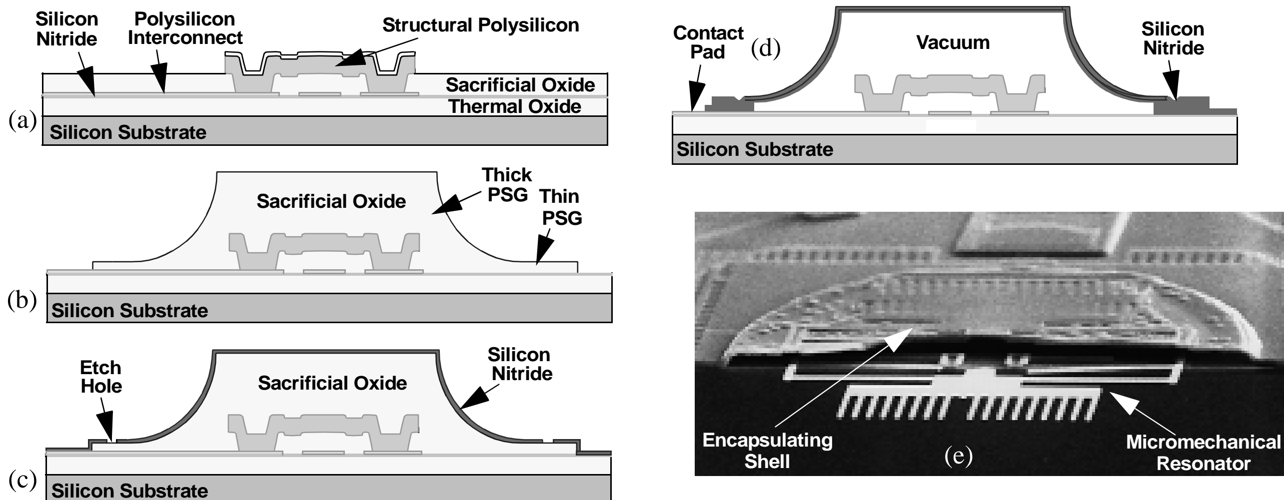

Fig. 26.Process flow for vacuum-encapsulation via surface-micromachining.[36] (a) Cross-section immediately after structural poly etch. (b) Deposit and pattern thick and thin PSG's in succession. (c) Deposit nitride and pattern etch holes. (d) Release structures, supercritical CO_2 dry. (d) Seal shell via nitride deposition, and open contacts to bond pads. (e) SEM of a broken shell, showing the previously encapsulated µmechanical resonator within.

may be difficult to achieve with a pre-circuits process because IC foundries may not permit "dirty" micromachined wafers into their ultra-clean fabrication facilities. Unfortunately, some amount of technical innovation is still needed before post-circuits processes become practical. The main difficulty has been that aluminum based circuit metallization technologies cannot withstand subsequent high temperature processing required by many micromechanics processes—especially those that must achieve high Q. Thus, compromises in either the circuits process or the micromechanics process have been necessary, undermining the overall modularity of the process. The MICS process[32] (Fig. 25), which used tungsten metallization instead of aluminum to withstand the high temperatures used in a following polysilicon surface micromachining module, is a good example of a post-circuits process. Research in this area is ongoing. The work to achieve nickel processes with adequate quality factor detailed in Section 5 is in fact partially driven by the desire to achieve a practical post-circuits process.

There are number of other processes that can to some extent be placed in more than one of the above categories. These include front bulk-micromachining processes similar to the single-crystal silicon process of Fig. 12 but using anisotropic wet etchants[34] and other processes that slightly alter conventional CMOS processes.[35] In addition, bonding processes, in which circuits and micromechanics are merged by bonding one onto the wafer of the other, are presently undergoing a resurgence. In particular, the advent of more sophisticated aligner-bonder instruments are now making possible much smaller bond pad sizes, which soon may enable wafer-level bonding with bond pad sizes small enough to compete with fully planar processed merging strategies in interface capacitance values. If the bond capacitance can indeed be lowered to this level with acceptable bonding yields, this technology would perhaps exhibit the most modularity of all.

7. ENCAPSULATION

From a broader perspective, the integration techniques discussed above are really methods for achieving low capacitance packaging of microelectromechanical systems. From the discussion in Section 2, another level of packaging is required to attain high Q vibrating µmechanical resonators: vacuum encapsulation. Although the requirement for vacuum is unique to vibrating µmechanical resonators, the requirement for encapsulation is nearly universal for all of the micromechanical devices discussed in this paper. In particular, some protection from the environment is necessary, if only to prevent contamination by particles (or even by molecules), or to isolate the device from electric fields or feedthrough currents.

The need for encapsulation is, of course, not confined to communications devices, but also extends to the vast majority of micromechanical applications, e.g., inertial navigation sensors. For many micromechanical applications, the cost of the encapsulation package can be a significant (often dominating) percentage of the total cost of the product. Thus, to reduce cost, packaging technologies with the highest yield and largest throughput are most desirable. Pursuant to this philosophy, wafer-level packaging approaches—some based on planar processing, some based on bonding—have been the focus of much research in recent years. Figure 26 presents cross-sections that summarize one approach to *wafer-level* vacuum encapsulation.[36] Although this and other encapsulation strategies have shown promise, there is still much room for improvement, especially given the

large percentage of total product cost attributed to the package alone. Research to reduce the cost (i.e., enhance the yield and throughput) of encapsulation technologies continues.

8. CONCLUSIONS

Micromechanical devices appear to be the perfect complements to active integrated circuit transistor devices in transceiver applications. In particular, transistor circuits excel at amplification, mixing, and digital processing, but are sorely deficient where frequency selectivity or high stability are required. Micromachined devices, on the other hand, excel at frequency selectivity and high stability, making them ideal components with which to fill the void in transceiver function left by transistors. These considerations in combination with the obvious similarities between micromachining and integrated circuit technologies—e.g., both are amenable to batch processing, both are based on wafer level deposition, lithography, and patterning—make an overwhelming case for research efforts aimed at merging the two technologies into a single wafer-level technology, perhaps someday capable of achieving a single-chip transceiver with all the sensitivity and link advantages of today's superheterodyne systems.

Is the application range for RF micromachining technologies confined to frequency selectivity and stability? Perhaps, not. Already, strategies for amplification, mixing, and digital processing via micromechanical means are under investigation, with the objective of lowering power dissipation by several times—a must for miniature transceivers, considering the tiny batteries that will be used to power them. In this respect, the micromachining technologies described in this paper and the improvements to be made in the near future may very well hold the key to future transceiver revolution.

9. ACKNOWLEDGMENTS

Aside from automatically acknowledging all referenced material within this overview article, the author gratefully acknowledges substantial contributions from former and present graduate students, in particular Kun Wang, Ark-Chew Wong, and Wan-Thai Hsu, who are largely responsible for the micromechanical resonator results. Research on micromechanical communications devices at the University of Michigan has been supported in part by grants from the Defense Advanced Research Projects Agency (DARPA), the National Science Foundation (NSF), NASA, and the Army Research Office (ARO), as well as numerous industrial sponsors.

10. REFERENCES

1. C. T.-C. Nguyen, L. P.B. Katehi, and G. M. Rebeiz, "Micromachined devices for wireless communications (invited)," *Proc. IEEE,* vol. 86, no. 8, pp. 1756-1768, Aug. 1998.
2. C. T.-C. Nguyen, "Micromechanical devices for wireless communications (invited)," *Proceedings*, 1998 IEEE International Workshop on Micro Electro Mechanical Systems, Heidelberg, Germany, Jan. 25-29, 1998, pp. 1-7.
3. F. D. Bannon III, J. R. Clark, and C. T.-C. Nguyen, "High frequency microelectromechanical IF filters," *Technical Digest*, IEEE International Electron Devices Meeting, San Francisco, CA, Dec. 8-11, 1996, pp. 773-776.
4. C. T.-C. Nguyen, "Frequency-selective MEMS for miniaturized communication devices (invited)," *Proceedings, 1*998 IEEE Aerospace Conference, Snowmass, Colorado, March 21-28, 1998, pp. 445-460.
5. K. Wang, F. D. Bannon III, J. R. Clark, and C. T.-C. Nguyen, "*Q*-enhancement of micromechanical filters via low-velocity spring coupling," to be published in the *Proceedings* of the 1997 IEEE International Ultrasonics Symposium, Toronto, Ontario, Canada, Oct. 5-8, 1997.
6. A. I. Zverev, *Handbook of Filter Synthesis*, New York: John Wiley & Sons, 1967.
7. C. T.-C. Nguyen and R. T. Howe, "Quality factor control for micromechanical resonators," *Technical Digest*, IEEE International Electron Devices Meeting, San Francisco, California, December 14-16, 1992, pp. 505-508.
8. W. E. Newell, "Miniaturization of tuning forks," *Science*, vol. 161, pp. 1320-1326, Sept. 1968.
9. K. Wang and C. T.-C. Nguyen, "High-order micromechanical electronic filters," *Proceedings*, 1997 IEEE International Micro Electro Mechanical Systems Workshop, Nagoya, Japan, Jan. 26-30, 1997, pp. 25-30.
10. W. C. Tang, T.-C. H. Nguyen, M. W. Judy, and R. T. Howe, "Electrostatic-comb drive of lateral polysilicon resonators," *Sensors and Actuators*, vol. A21-23, pp. 328-331. 1990.
11. W.-T. Hsu and C. T.-C. Nguyen, "Geometric stress compensation for enhanced thermal stability in micromechanical resonators," to be published in the *Proceedings* of the 1998 IEEE International Ultrasonics Symposium, Sendai, Japan, Oct. 5-8, 1998.
12. T. A. Core, W. K. Tsang, S. J. Sherman, "Fabrication technology for an integrated surface-micromachined sensor," *Solid State Technology*, pp. 39-47, Oct. 1993.
13. J. W. Weigold and S. W. Pang, "A New Frontside-Release Etch-Diffusion Process for the Fabrication of Thick Si Micro-

structures", *Proc*. 9th Int. Conference on Solid State Sensors and Actuators (Transducers'97), Chicago, June 1997, pp. 1435-1438.

14. E. E. Hui, C. G. Keller, R. T. Howe, "Carbonized parylene as a conformal sacrificial layer," *Technical Digest*, 1998 Solid-State Sensor and Actuator Workshop, Hilton Head, SC, June 3-6, 1998, pp. 256-260.
15. S. V. Krishnaswamy, J. Rosenbaum, S. Horwitz, C. Yale, and R. A. Moore, "Compact FBAR filters offer low-loss performance," *Microwaves & RF*, pp. 127-136, Sept. 1991.
16. A. N. Cleland and M. L. Roukes, "Fabrication of high frequency nanometer scale mechanical resonators from bulk Si crystals," *Appl. Phys. Lett.*, **69** (18), pp. 2653-2655, Oct. 28, 1996.
17. N. Slawsby, "Frequency control requirements of radar," *Proceedings* of the 1994 IEEE International Frequency Control Symposium, June 1-3, 1994, pp. 633-640.
18. J. W. Weigold, A.-C. Wong, C. T.-C. Nguyen, and S. W. Pang, "Thick single crystal Si lateral resonant devices integrated with a conventional circuit process", *Late News Supplemental Digest*, 1988 Solid State Sensor and Actuator Workshop, Hilton Head, South Carolina, June 8-11, 1998, pp. 15-16.
19. G. T. A. Kovacs, N. I. Maluf, K. E. Petersen, "Bulk micromachining of silicon," *Proc. IEEE*, vol. 86, no. 8, pp. 1536-1551, Aug. 1998.
20. A. R. Brown and G. M. Rebeiz, "Micromachined micropackaged filter banks", *Microwave and Guided Wave Letters*, vol. 8, pp. 158-160, March 1998.
21. G. M. Rebeiz, D. P. Kasilingam, Y. Guo, P. A. Stimpson, and D. B. Rutledge, "Monolithic millimeter-wave two-dimensional horn imaging arrays," *IEEE Trans. Antennas Propagat.*, vol. AP-38, pp. 1473-1482, Sept. 1990.
22. G. P. Gauthier, A. Courtay, and G. M. Rebeiz, "Microstrip antennas on synthesized low dielectric constant substrates," *IEEE Trans. Antennas Propag.*, vol. AP-45, pp. 1310-1314, Aug. 1997.
23. B. Ziaie, N. K. Kocaman, and K. Najafi, "A generic micromachined silicon platform for low-power, low-loss miniature transceivers," *Digest of Technical Papers*, 1997 International Conference on Solid-State Sensors and Actuators (Transducers'97), Chicago, Illinois, June 16-19, 1997, pp. 257-260.
24. H. Nathanson, W. E. Newell, R. A. Wickstrom, and J. R. Davis, Jr., "The resonant gate transistor," *IEEE Trans. Electron Devices*, vol. ED-14, No. 3, pp. 117-133, March 1967.
25. D. J. Young, V. Malba, J.-J. Ou, A. F. Bernhardt, and B. E. Boser, "Monolithic high-performance three-dimensional coil inductors for wireless communication applications," *Technical Digest*, IEEE International Electron Devices Meeting, Washington, D. C., Dec. 8-11, 1997, pp. 67-70.
26. D. J. Young and B. E. Boser, "A micromachined variable capacitor for monolithic low-noise VCOs," *Technical Digest*, 1996 Solid-State Sensor and Actuator Workshop, Hilton Head Island, South Carolina, June 3-6, 1996, pp. 86-89.
27. C. Goldsmith, J. Randall, S. Eshelman, T. H. Lin, D. Denniston, S. Chen and B. Norvell, "Characteristics of micromachined switches at microwave frequencies," *IEEE MTT-S Digest*, June, 1996, pp. 1141-1144.
28. S. Pacheco, C. T.-C. Nguyen, and L. P. B. Katehi, "Micromechanical electrostatic K-band switches," *Proceedings,* IEEE MTT-S International Microwave Symposium, Baltimore, Maryland, June 7-12, 1998, pp. 1569-1572.
29. C. T.-C. Nguyen and R. T. Howe, "Microresonator frequency control and stabilization using an integrated micro oven," *Digest of Technical Papers*, the 7th International Conference on Solid-State Sensors and Actuators (Transducers'93), Yokohama, Japan, June 7-10, 1993, pp. 1040-1043.
30. C. T.-C. Nguyen, "Communications applications of microelectromechanical systems (invited)," to be published in the *Proceedings* of Sensors Expo, San Jose, California, May 20, 1998.
31. J. H. Smith, S. Montague, J. J. Sniegowski, J. R. Murray, *et al*., "Embedded micromechanical devices for the monolithic integration of MEMS with CMOS," *Proceedings*, IEEE International Electron Devices Meeting, Washington, D.C., Dec. 10-13, 1995, pp. 609-612.
32. J. M. Bustillo, G. K. Fedder, C. T.-C. Nguyen, and R. T. Howe, "Process technology for the modular integration of CMOS and polysilicon microstructures," *Microsystem Technologies*, **1** (1994), pp. 30-41.
33. C. T.-C. Nguyen and R. T. Howe, "CMOS Micromechanical Resonator Oscillator," *Technical Digest*, IEEE International Electron Devices Meeting, Washington, D. C., December 5-8, 1993, pp. 199-202.
34. H. Baltes, O. Paul, and O. Brand, "Micromachined thermally based CMOS microsensors," *Proc. IEEE*, vol. 86, no. 8, pp. 1660-1678, Aug. 1998.
35. G. K. Fedder, S. Santhanam, M. L. Reed, S. C. Eagle, D. F. Guillou, M. S.-C. Lu, and L. R. Carley, "Laminated high-aspect-ratio microstructures in a conventional CMOS process," *Sensors and Actuators*, vol. A57, no. 2, pp. 103-110, March 1997.
36. L. Lin, K. M. McNair, R. T. Howe, and A. P. Pisano, "Vacuum-encapsulated lateral microresonators," *Digest of Technical Papers*, the 7th International Conference on Solid-State Sensors and Actuators (Transducers'93), Yokohama, Japan, June 7-10, 1993, pp. 270-273.